Hybrid diamond-silicon angular-dispersive x-ray monochromator with 0.25-meV energy bandwidth and high spectral efficiency

S. Stoupin,[1,*] Y. V. Shvyd'ko,[1] D. Shu,[1] V. D. Blank,[2] S. A. Terentyev,[2] S. N. Polyakov,[2,3] M. S. Kuznetsov,[2] I. Lemesh,[2] K. Mundboth,[4] S. P. Collins,[4] J. P. Sutter,[4] and M. Tolkiehn[5]

[1]*Advanced Photon Source, Argonne National Laboratory, Illinois, USA*
[2]*Technological Institute for Superhard and Novel Carbon Materials, Troitsk, Moscow, Russia*
[3]*Skobeltsyn Institute of Nuclear Physics, Lomonosov Moscow State University, Moscow, Russia*
[4]*Diamond Light Source, Oxford, UK*
[5]*Deutsches Elektronen-Synchrotron, Hamburg, Germany*
[*]*sstoupin@aps.anl.gov*

Abstract: We report on the design, implementation, and performance of an x-ray monochromator with ultra-high energy resolution ($\Delta E/E \simeq 2.7 \times 10^{-8}$) and high spectral efficiency using x rays with photon energies $E \simeq 9.13$ keV. The operating principle of the monochromator is based on the phenomenon of angular dispersion in Bragg back-diffraction. The optical scheme of the monochromator is a modification of a scheme reported earlier [Shvyd'ko et al., Phys. Rev. A **84**, 053823 (2011)], where a collimator/wavelength selector Si crystal was replaced with a 100-μm-thick type IIa diamond crystal. This modification provides a very-small-energy bandwidth $\Delta E \simeq 0.25$ meV, a 3-fold increase in the aperture of the accepted beam, a reduction in the cumulative angular dispersion rate of x rays emanating from the monochromator for better focusing on a sample, a sufficient angular acceptance matching the angular divergence of an undulator source (≈ 10 μrad), and an improved throughput due to low x-ray absorption in the thin diamond crystal. The measured spectral efficiency of the monochromator was $\approx 65\%$ with an aperture of 0.3×1 mm^2. The performance parameters of the monochromator are suitable for inelastic x-ray spectroscopy with an absolute energy resolution $\Delta E < 1$ meV.

OCIS codes: (120.4140) Monochromators; (340.6720) Synchrotron radiation; (300.6560) Spectroscopy, x-ray; (230.1480) Bragg reflectors; (220.1920) Diamond machining.

References and links

1. E. Burkel, "Phonon spectroscopy by inelastic x-ray scattering," Rep. Prog. Phys. **63**, 171 (2000).
2. H. Sinn, "Spectroscopy with meV energy resolution," J. Phys.: Condens. Matter **13**, 7525–7537 (2001).
3. M. Krisch and F. Sette, *Light Scattering in Solids IX* (Springer, Berlin, 2007), vol. 108 of *Topics in Applied Physics*, chap. Inelastic X-Ray Scattering from Phonons, pp. 317–370.
4. E. Gerdau and H. de Waard, eds., *Nuclear Resonant Scattering of Synchrotron Radiation* (Baltzer, 1999/2000). Special issues of the *Hyperfine Interact.*, Vol. 123-125.

#197351 - $15.00 USD Received 16 Sep 2013; revised 30 Oct 2013; accepted 1 Nov 2013; published 9 Dec 2013

5. R. Röhlsberger, *Nuclear Condensed Matter Physics with Synchrotron Radiation. Basic Principles, Methodology and Applications*, vol. 208 of *Springer Tracts in Modern Physics* (Springer Verlag, Berlin-Heidelberg, 2004).
6. H.-C. Wille, Y. V. Shvyd'ko, E. Gerdau, M. Lerche, M. Lucht, H. D. Rüter, and J. Zegenhagen, "Anomalous isotopic effect on the lattice constant of silicon," Phys. Rev. Lett. **89**, 285901 (2002).
7. M. Y. Hu, H. Sinn, A. Alatas, E. E. Alp, W. Sturhahn, H.-C. Wille, Y. V. Shvyd'ko, J. P. Sutter, J. Bandaru, E. E. Haller, V. I. Ozhogin, S. Rodrigues, R. Colella, E. Kartheuser, and M. A. Villert, "The effect of isotopic composition on the lattice parameter of germanium," Phys. Rev. B **67**, 113306 (2003).
8. S. Stoupin and Y. V. Shvyd'ko, "Thermal expansion of diamond at low temperatures," Phys. Rev. Lett. **104**, 085901 (2010).
9. M. Yabashi, K. Tamasaku, and T. Ishikawa, "Measurement of x-ray pulse widths by intensity interferometry," Phys. Rev. Lett. **88**, 244801 (2002).
10. Y. Shvyd'ko, *X-Ray Optics – High-Energy-Resolution Applications*, vol. 98 of *Optical Sciences* (Springer, Berlin Heidelberg New York, 2004).
11. M. Yabashi, K. Tamasaku, S. Kikuta, and T. Ishikawa, "An x-ray monochromator with an energy resolution of 8×10^{-9} at 14.4 keV," Rev. Sci. Instrum. **72**, 4080 (2001).
12. R. Verbeni, F. Sette, M. Krisch, U. Bergmann, B. Gorges, C. Halcoussis, K. Martel, C. Masciovecchio, J. F. Ribois, G. Ruocco, and H. Sinn, "X-ray monochromator with 2×10^{-8} energy resolution," J. Synchrotron Rad. **3**, 62–64 (1996).
13. T. S. Toellner, A. Alatas, and A. H. Said, "Six-reflection meV-monochromator for synchrotron radiation," J. Synchrotron Rad. **18**, 605–611 (2011).
14. T. Matsushita and U. Kaminaga, "A systematic method of estimating the performance of X-ray optical systems for synchrotron radiation. II. Treatment in position-angle–wavelength space," J. Appl. Crystallogr. **13**, 472–478 (1980).
15. S. Brauer, G. B. Stephenson, and M. Sutton, "Perfect Crystals in the Asymmetric Bragg Geometry as Optical Elements for Coherent X-ray Beams," J. Synchrotron Rad. **2**, 163–173 (1995).
16. Y. V. Shvyd'ko, M. Lerche, U. Kuetgens, H. D. Rüter, A. Alatas, and J. Zhao, "X-ray bragg diffraction in asymmetric backscattering geometry," Phys. Rev. Lett. **97**, 235502 (2006).
17. Y. V. Shvyd'ko, U. Kuetgens, H. D. Rüter, M. Lerche, A. Alatas, and J. Zhao, "Progress in the development of new optics for very high resolution inelastic x-ray scattering spectroscopy," AIP Conf. Proc. **879**, 737–745 (2007).
18. Y. Shvyd'ko, S. Stoupin, D. Shu, and R. Khachatryan, "Using angular dispersion and anomalous transmission to shape ultramonochromatic x rays," Phys. Rev. A **84**, 053823 (2011).
19. Y. Shvyd'ko, S. Stoupin, K. Mundboth, and J. Kim, "Hard-x-ray spectrographs with resolution beyond 100 μev," Phys. Rev. A **87**, 043835 (2013).
20. Y. Q. Cai, D. S. Coburn, A. Cunsolo, J. W. Keister, M. G. Honnicke, X. R. Huang, C. N. Kodituwakku, Y. Stetsko, A. Suvorov, N. Hiraoka, K. D. Tsuei, and H. C. Wille, "The ultrahigh resolution IXS beamline of NSLS-II: Recent advances and scientific opportunities," J. Phys.: Conf. Ser. **425**, 202001 (2013).
21. Y. Shvyd'ko, "Enhanced x-ray angular dispersion and x-ray spectrographs with resolving power beyond 10^8," Proc. SPIE, Advances in X-Ray/EUV Optics and Components VII **8502**, 85020J (2012).
22. A. Souvorov, M. Drakopoulos, I. Snigireva, and A. Snigirev, "Asymmetrically cut crystals as optical elements for coherent x-ray beam conditioning," J. Phys. D: Appl. Phys. **32**, A184A192 (1999).
23. V. G. Kohn, A. I. Chumakov, and R. Rüffer, "Wave theory of focusing monochromator of synchrotron radiation," J. Synchrotron Rad. **16**, 635–641 (2009).
24. X. R. Huang, A. T. Macrander, M. G. Honnicke, Y. Q. Cai, and P. Fernandez, "Dispersive spread of virtual sources by asymmetric X-ray monochromators," J. Appl. Cryst. **45**, 255262 (2012).
25. R. C. Burns, A. I. Chumakov, S. H. Connell, D. Dube, H. P. Godfried, J. O. Hansen, J. Hrtwig, J. Hoszowska, F. Masiello, L. Mkhonza, M. Rebak, A. Rommevaux, R. Setshedi, and P. V. Vaerenbergh, "HPHT growth and x-ray characterization of high-quality type IIa diamond," J. Phys.: Condens. Matter **21**, 364224 (2009).
26. S. Polyakov, V. Denisov, N.V.Kuzmin, M. Kuznetsov, S. Martyushov, S. Nosukhin, S. Terentiev, and V. Blank, "Characterization of top-quality type IIa synthetic diamonds for new x-ray optics," Diamond Relat. Mater. **20**, 726 – 728 (2011).
27. H. Sumiya and K. Tamasaku, "Large defect-free synthetic type IIa diamond crystals synthesized via high pressure and high temperature," Jpn. J. Appl. Phys. **51**, 090102 (2012).
28. Y. V. Shvyd'ko, S. Stoupin, V. Blank, and S. Terentyev, "Near 100% Bragg reflectivity of X-rays," Nat. Photonics **5**, 539 (2011).
29. J. Amann, W. Berg, V. Blank, F.-J. Decker, Y. Ding, P. Emma, Y. Feng, J. Frisch, D. Fritz, J. Hastings, Z. Huang, J. Krzywinski, R. Lindberg, H. Loos, A. Lutman, H.-D. Nuhn, D. Ratner, J. Rzepiela, D. Shu, Y. Shvyd'ko, S. Spampinati, S. Stoupin, S. Terentiev, E. Trakhtenberg, D. Walz, J. Welch, J. Wu, A. Zholents, and D. Zhu, "Demonstration of self-seeding in a hard-X-ray free-electron laser," Nat. Photonics **6**, 693–698 (2012).
30. S. Stoupin, V. Blank, S. Terentyev, S. Polyakov, V. Denisov, M. Kuznetsov, Y. Shvyd'ko, D. Shu, P. Emma, J. Maj, and J. Katsoudas, "Diamond crystal optics for self-seeding of hard X-rays in X-ray free-electron lasers," Diamond Relat. Mater. **33**, 1 – 4 (2013).

#197351 - $15.00 USD Received 16 Sep 2013; revised 30 Oct 2013; accepted 1 Nov 2013; published 9 Dec 2013

31. D. Shu, S. Stoupin, R. Khachatryan, K. Goetze, T. Roberts, and Y. Shvyd'ko, "Optomechanical design of ultrahigh-resolution monochromator and analyzer for inelastic x-ray scattering spectrometer at the Advanced Photon Source," Proc. SPIE: Optomechanics **8125**, 812507 (2011).
32. D. Shu, S. Stoupin, R. Khachatryan, K. A. Goetze, T. Roberts, K. Mundboth, S. Collins, and Y. Shvyd'ko, "Precision mechanical design of an ultrahigh-resolution inelastic x-ray scattering spectrometer system with CDFDW optics at the APS," J. Phys: Conf. Ser. **425**, 052031 (2013).
33. D. Shu, Y. Shvydko, S. Stoupin, R. Khachatryan, K. Goetze, and T. Roberts, "Precision mechanical structure of an ultra-high-resolution spectrometer for inelastic x-ray scattering instrument," 13551788, U.S. patent pending (2012).
34. T. Toellner, "Monochromatization of synchrotron radiation for nuclear resonant scattering experiments," Hyperfine Interact. **125**, 3–28 (2000).
35. A. I. Chumakov, R. Rüffer, O. Leupold, A. Barla, H. Thiess, T. Asthalter, B. P. Doyle, A. Snigirev, and A. Q. R. Baron, "High-energy-resolution x-ray optics with refractive collimators," Appl. Phys. Lett. **77**, 31–33 (2000).
36. T. S. Toellner, A. Alatas, A. Said, D. Shu, W. Sturhahn, and J. Zhao, "A cryogenically stabilized meV-monochromator for hard X-rays," J. Synchrotron Rad. **13**, 211–215 (2006).
37. T. S. Toellner, A. Alatas, and A. H. Said, "Six-reflection meV-monochromator for synchrotron radiation," J. Synchrotron Rad. **18**, 605–611 (2011).
38. S. Stoupin, Y. Shvyd'ko, D. Shu, R. Khachatryan, X. Xiao, F. DeCarlo, K. Goetze, T. Roberts, C. Roehrig, and A. Deriy, "Hard x-ray monochromator with milli-electron volt bandwidth for high-resolution diffraction studies of diamond crystals," Rev. Sci. Instrum. **83**, 023105 (2012).
39. Y. Feng, R. Alonso-Mori, V. Blank, S. Boutet, M. Chollet, T. B. van Driel, D. M. Fritz, J. M. Glownia, J. B. Hastings, H. Lemke, M. Messerchmidt, P. A. Montanez, A. Robert, J. Robinson, L. Samoylova, Y. Shvydko, M. Sikorski, H. Sinn, S. Song, V. N. Srinivasan, S. Stoupin, S. Terentiev, G. Williams, and D. Zhu, "Recent development of thin diamond crystals for x-ray FEL beam-sharing," Proc. SPIE, Advances in X-ray Free-Electron Lasers II: Instrumentation **8778**, 87780B (2013).

1. Introduction

High-resolution x-ray monochromators for hard x-rays ($E \simeq 10-20$ keV) with energy bandwidths $\Delta E \simeq 1-0.1$ meV are indispensable tools for inelastic x-ray scattering (IXS) spectroscopy [1–3], nuclear resonant scattering spectroscopy [4, 5], ultra-precise crystal lattice parameter measurements [6–8], x-ray interferometry [9], x-ray metrology, and for other applications in x-ray science. Different monochromator designs utilize common principles of x-ray crystal optics (see [10] for a review). Monochromatization to bandwidths as small as $\simeq 0.13$ meV has been demonstrated [11], however, with a low efficiency of a few percent. High-efficiency $\simeq 40-70\%$ can be achieved in monochromatization to bandwidths $\simeq 1-0.8$ meV [12, 13]. Here we present a hard x-ray monochromator with a unique combination of a very small 0.25-meV bandwidth, a very high 65% efficiency, and steep spectral tails. The monochromator is designed for applications in ultra-high-resolution IXS; however, it can be used in other research fields as well.

The operating principle of the monochromator is based on the effect of angular dispersion in Bragg diffraction from asymmetrically cut crystals [10, 14–16]. The basic implementation of angular dispersive (AD) x-ray optics involves three major functional crystal elements: a collimator (C), a dispersive element (D), and a wavelength selector (W). The C element collimates the incident x-ray beam. The D element transforms the spectral spread of x rays into an angular spread. The W element acts as a wavelength selector, selecting the waves within a desired angular, and thus spectral, interval [10, 16].

Angular dispersive x-ray optics can achieve sub-meV bandwidths, a very large angular acceptance of $\simeq 100$ μrad, and steep tails of the spectral functions. The realized previous AD optical schemes [16–20] are highly suitable as analyzers for IXS spectrometers [10]. Spectral efficiencies of $\approx$ 16-20% were demonstrated.

In this work we show that design of AD optics can be optimized to yield x-ray monochromators with an unmatched performance in terms of spectral efficiency and energy resolution characteristics. The demonstrated efficiency and superior spectral properties render AD x-ray monochromators perfectly suitable for IXS with very-high-energy resolution.

#197351 - $15.00 USD Received 16 Sep 2013; revised 30 Oct 2013; accepted 1 Nov 2013; published 9 Dec 2013

The paper is organized as follows: In Sec. 2, we briefly describe previously demonstrated AD optics, and how it can be modified to a highly efficient hybrid silicon-diamond monochromator. In Sec. 3, details of the design and theoretical simulations of the spectral properties of the monochromator are presented. Experimental details are given in Sec. 4. Sections 5, 6, and 7 describe performance characteristics of the monochromator. The design and measured performance parameters are summarized in Sec. 8.

2. From CDFDW to hybrid CDDW optics

The recent implementation of an AD optical unit [18,19] to obtain highly monochromatic x rays with unique spectral properties includes three single crystals as shown in Fig. 1. The first crystal (CFW) plays the role of a collimator (C) upon the first asymmetric Bragg reflection, a filter (F) in transmission due to the anomalously high transmission effect, and a wavelength selector (W). After the first reflection the collimated x-ray beam is incident on a strongly asymmetric second crystal D_1, which acts as a dispersive element (D). A portion of the dispersion fan emanating from D_1 enters the anomalous condition for transmission through the CFW crystal. This portion is further dispersed by a second dispersive element D_2 (identical to D_1) with doubled angular dispersion rate and subsequently reflected from the CFW crystal, now performing the function of the wavelength selector. Thus, this particular implementation of AD optics has an acronym CDFDW.

Unlike conventional diffracting optics, the spectral bandwidth of AD optics does not directly relate to intrinsic energy widths of Bragg reflections [10]. DuMond diagram analysis yields the following estimate for the spectral bandwidth of the CDFDW unit [18]:

$$\frac{\Delta E}{E} = \frac{\Delta\theta'_C + \Delta\theta_W}{4\tan\eta_D}, \tag{1}$$

where $\Delta\theta'_C$ is the angular divergence of x rays after the collimator, $\Delta\theta_W$ is the angular acceptance of the wavelength selector, and η_D is the asymmetry angle of the D crystals (angle between the reflecting atomic planes and the crystal surface).

The particular design of the CDFDW optics presented in [18] is advantageous for an analyzer. The large asymmetry of the Bragg reflection from the CFW crystal results in the favorable combination, first, of the large angular acceptance enabled by the C reflection; second, of anomalous transmission, enabled by the F transmission; and third, of the small bandwidth, enabled by the W reflection. However, this design is not optimal for a monochromator. The use of highly asymmetric reflections results in serious drawbacks. First, the large asymmetry in the C reflection increases the size of the reflected beam and requires very long D crystals to accept the entire beam. Second, due to its large asymmetry the W reflection enhances dramatically the cumulative angular dispersion rate of the entire system [19, 21]. Angular dispersion due to asymmetric reflections changes the position of the virtual source and, therefore, may significantly impair focusing of x rays on the sample after the monochromator [22–24].

These problems can be mitigated and the CDFDW design can be better adopted for monochromator applications using higher indexed Bragg reflection of the CFW crystal with reduced asymmetry. This can still provide sufficient angular acceptance of the optics for the incident beam from an undulator source with a $\simeq 10-15$-μrad angular divergence and enable very high spectral resolution by keeping $\Delta\theta'_C$ and $\Delta\theta_W$ small (see Eq. (1)). However, the reduced asymmetry will deteriorate anomalous transmission and thus efficiency of the CDFDW optics. The problem can be solved by avoidance of the anomalous transmission condition while using a low-absorbing crystal material, such as diamond, to substantially reduce losses in transmission. Recent advances in fabrication of high-quality diamond crystals and their use in high-resolution, low-loss x-ray optics [25–30] enable practical realization of this approach.

#197351 - $15.00 USD Received 16 Sep 2013; revised 30 Oct 2013; accepted 1 Nov 2013; published 9 Dec 2013

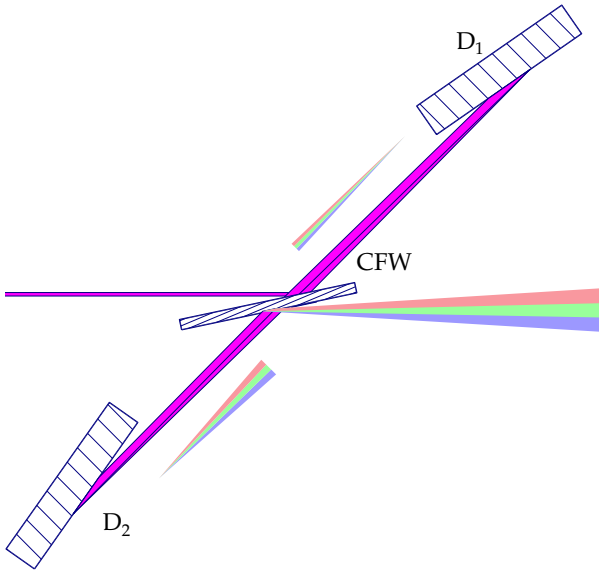

Fig. 1. Scheme of the previously implemented CDFDW optics [18, 19]. The first crystal (CFW) plays the role of a collimator (C) upon the first asymmetric Bragg reflection, an anomalous transmission filter (F), and a wavelength selector (W). After the first reflection the collimated x-ray beam is incident on a strongly asymmetric second crystal D_1. The x-ray beam reflected from D_1 enters the condition for anomalously high transmission through the CFW crystal. The transmitted beam is further dispersed by a second dispersive element D_2 with doubled angular dispersion rate and subsequently reflected from the CFW crystal, now performing the function of the wavelength selector. The effect of angular dispersion at the exit of the CDFDW optics is illustrated by an exaggerated divergent fan where photons of different energies propagate at different reflection angles. Only angular dispersion of the exit beam is shown for clarity.

In the following it is demonstrated that use of a thin diamond crystal with a special asymmetry as a collimator/wavelength-selector in AD x-ray optics yields a high-energy-resolution monochromator with an unmatched performance at an intermediate hard x-ray energy ($\approx$ 9 keV). With such an operating energy, the monochomator is perfectly suitable to both high- and medium-energy storage-ring synchrotron radiation facilities, as well as x-ray free-electron lasers (XFEL). The reduced x-ray absorption in the collimator/wavelength selector results in a substantial improvement in the spectral efficiency of the monochromator ($\simeq$ 65%) and in the absence of the anomalous transmission condition (at the expense of some broadening in the tails of the spectral resolution function). The modified monochromator has a narrower spectral bandwidth of $\simeq$ 0.25 meV due to the optimized angular acceptance/divergence characteristics and a reduced angular dispersion rate of the monochromatized x rays for better focusing on a sample. Due to absence of the anomalous transmission the monochromator can be used away from the exact backscattering geometry, thus avoiding potential problems with intensity losses due to multiple Bragg diffraction.

3. Design and theory

The optomechanical scheme of the monochromator in the dispersion plane is shown in Fig. 2(a). Figure 2(b) is a three-dimensional representation of the path of the x-ray beam through the

#197351 - $15.00 USD Received 16 Sep 2013; revised 30 Oct 2013; accepted 1 Nov 2013; published 9 Dec 2013

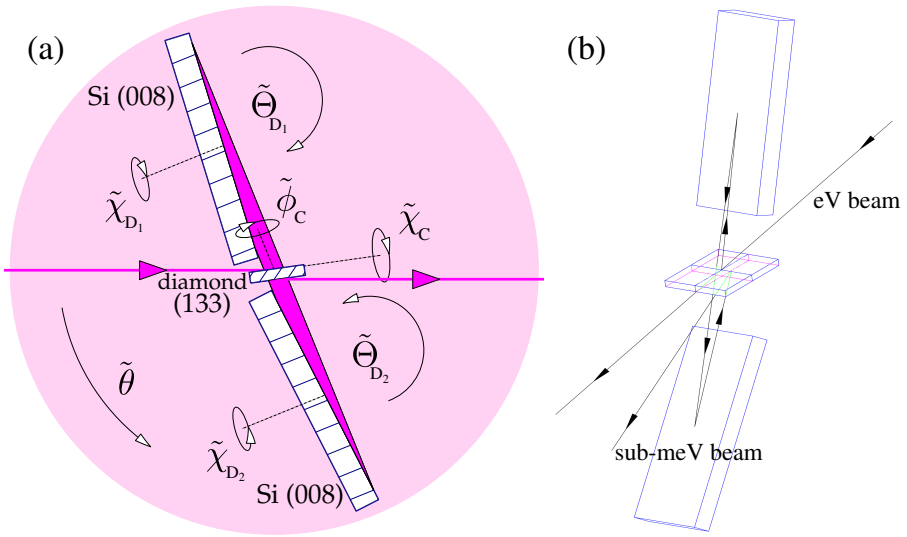

Fig. 2. (a) Optomechanical scheme of the monochromator (see text for details); (b) a three-dimensional representation of the path of the x-ray beam through the monochromator.

monochromator. The scheme comprises three diffracting crystals and five consecutive interactions of x rays via particular Bragg diffraction conditions. The implemented angular degrees of freedom are shown by rotation arrows. The angular degrees of freedom in the dispersion plane (a plane composed by the reciprocal vectors of the participating Bragg reflections and normals to the crystal surfaces) are denoted as $\tilde{\theta}$, $\tilde{\Theta}_{D_1}$, and $\tilde{\Theta}_{D_2}$. Note that the angle $\tilde{\theta}$ corresponds to rotation of the entire optical assembly in the dispersion plane. The other angular degrees of freedom $\tilde{\chi}_{D_1}$, $\tilde{\chi}_{D_2}$, $\tilde{\chi}_C$, and $\tilde{\phi}_C$ represent rotation of crystals in the planes perpendicular to the dispersion plane. These angular motions facilitate optical alignment of the monochromator.

An x-ray beam from a double-crystal, high-heat-load pre-monochromator (not shown in the figure) with an energy bandwidth of $\Delta E_X \simeq 0.57$ eV and with an angular divergence of the undulator source (≈ 10 μrad) is incident on a diamond CW crystal. The diamond 133 Bragg reflection with an asymmetry angle $\eta_C = 48^\circ$ is utilized. In the first interaction the diamond crystal plays the role of a collimator. The reflected beam collimated by the asymmetric diamond 133 reflection is incident on a dispersing element D_1 [Si (008) crystal with a large asymmetry angle $\eta_D = 88^\circ$]. The Bragg reflection from D_1 in the vicinity of the exact backscattering condition produces an angular dispersed x-ray beam (dispersion fan) where different reflection angles correspond to different photon energies. In the third interaction the dispersion fan is transmitted through the diamond crystal with little absorption.

We note that unlike the CDFDW optics, there is no substantial enhancement of the transmitted intensity in the anomalous transmission condition due to low x-ray absorption and smaller asymmetry of the diamond crystal. Thus, transmission through the diamond crystal does not perform the function of a spectral filter F and an appropriate acronym for the monochromator is therefore CDDW.

In the fourth interaction the dispersion fan transmitted through the diamond crystal is reflected from D_2 element, which is identical to D_1. This enhances the angular dispersion by a factor of two. In the final fifth step, a small fraction of the dispersion fan emanating from D_2 crystal; is reflected from the diamond crystal, which now plays the role of the wavelength selector (W). This results in a dramatic reduction in the spectral bandwidth. The described interac-

#197351 - $15.00 USD Received 16 Sep 2013; revised 30 Oct 2013; accepted 1 Nov 2013; published 9 Dec 2013

tions are illustrated below using theoretical calculations of energy-dependent x-ray reflectivity. Crystal parameters used in the calculations are given in Table 1.

Table 1. Elements of the CDDW optics and their crystal and Bragg reflection parameters as used in all dynamical theory calculations and in the experiment: h,k,l, Miller indices of the Bragg diffraction vector $\boldsymbol{H}$; η_H, asymmetry angle; θ_H, glancing angle of incidence; $b_H = -\sin(\theta_H \pm \eta_H)/\sin(\theta_H \mp \eta_H)$, asymmetry ratio; $\Delta E_H^{(s)}$ and $\Delta\theta_H^s$, Bragg's reflection intrinsic spectral width and angular acceptance in symmetric scattering geometry, respectively; and d, crystal thickness. X-ray photon energy E = 9.1315 keV.

Crystal/ function	$\boldsymbol{H}$ (hkl)	η_H (deg)	θ_H (deg)	b_H	ΔE_H^s (meV)	$\Delta\theta_H^s$ (μrad)	d (mm)
CW/C	133	48.0	56.1	-0.145	39.9	6.5	0.1
$D_{1,2}$/D	008	88.0	89.9	-1.1	25	1870	20
CW/W	133	48.0	56.1	-6.9	39.9	6.5	0.1

Figure 3 shows the energy dependence of reflectivity calculated using the dynamical theory of x-ray diffraction from crystals upon each consecutive interaction in the monochromator. The origin of the energy scale corresponds to the backscattering energy $E_0 \simeq 9.1315$ keV of the Si 008 reflection with the asymmetry angle $\eta_D = 88^\circ$. The calculations were performed in the two-beam approximation under the assumption that the reciprocal vectors of all Bragg reflections lie in the dispersion plane. The silicon and diamond crystals were assumed to be perfect crystals at a temperature of 300 K. A Gaussian angular distribution with a standard deviation of 5 μrad was assumed for the incident beam. Angular offsets of 200 μrad from the exact back-scattering angles to the D crystals were used in the calculations. According to the theory, the energy bandwidth of the monochromator is $\Delta E_M \simeq 0.246$ meV (full width at half maximum or FWHM) and the peak throughput (maximum reflectivity) is $T \simeq 58\%$. We note that Eq. (1) yields $\Delta E_M \simeq 0.39$ meV, which is a slight overestimation of the energy bandwidth typical for DuMond analysis [10]. However, this estimate is very helpful in the design of AD optics since it demonstrates functioning of the optics and provides an estimate for the energy bandwidth.

For comparison, a Gaussian function of the same energy width (FWHM) is plotted in Fig. 3 (dashed line) as an example of a distribution with steep tails. We note that unlike the CDFDW optics [18], the absence of anomalous transmission in the design of the monochromator does not allow us to approach the tails of the Gaussian distribution over several orders of magnitude in theory. Nevertheless, the resulting tails of the spectral resolution function are much steeper than those of a Lorentzian distribution found in conventional backscattering optics.

Another important characteristic of AD optics is the cumulative angular dispersion rate of the output x-ray beam. For optics used as a monochromator, this angular dispersion rate should be minimized to avoid defocusing of x rays on the sample [22–24]. The opposite situation of a large cumulative dispersion rate is particularly beneficial for the analyzer, which enables hard x-ray spectrographs [19].

The cumulative dispersion rate of the CDDW optics can be estimated as $\mathscr{D}_\cup \simeq 2b_W\mathscr{D}_D$ [19]. In the present case, the asymmetry ratio of the wavelength selector is b_W = -6.92 and the dispersion rate of the D-crystal is $\mathscr{D}_D \simeq 6.27$ μrad/meV . Thus, $\mathscr{D}_\cup \simeq -87$ μrad/meV. This value is about three times less than the value of -314 μrad/meV demonstrated earlier for the CDFDW unit having a Si (022) CFW-crystal with a greater asymmetry ratio b_W [19].

If x rays emanating from the monochromator are focused on a sample using an optical focusing element with a focal distance of $f \approx 1$ m, the minimum possible size of the focal spot will be $\Delta x = f\mathscr{D}_\cup\Delta E_M \approx 20$ μm. This is consistent with design values for inelastic x-ray spec-

#197351 - $15.00 USD Received 16 Sep 2013; revised 30 Oct 2013; accepted 1 Nov 2013; published 9 Dec 2013

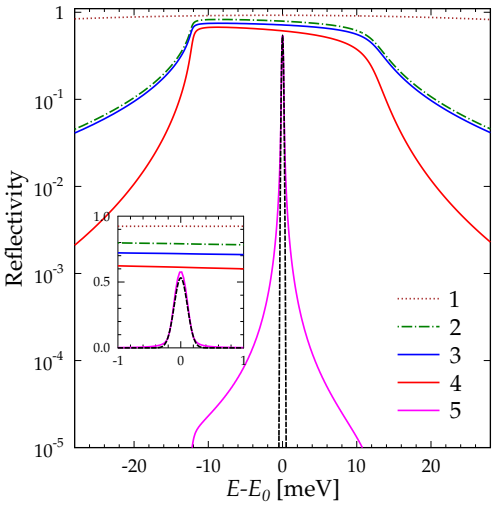

Fig. 3. Dynamical theory calculations of the spectral distribution of x rays after each successive reflection indicated by number and color, from the crystals of the angular dispersive monochromator. Black dashed line shows a Gaussian distribution of the same full width at half maximum. The insert shows the same distributions on the linear scale in the vicinity of the Si 008 backscattering energy E_0.

trometers.

Finally, due to a reduced asymmetry ratio of the CW crystal, the vertical size of the beam accepted by the monochromator is increased in comparison to that of the CDFDW unit if the length of the D crystal remains unchanged. The 3-fold increase results from the choice of the CW Bragg reflection with the b_W asymmetry ratio reduced by a factor of 3. The vertical acceptance estimated using simple geometrical considerations is

$$s = \frac{L}{b_W} \sin(\theta_C + \eta_C) \simeq 0.46 \text{ mm}, \tag{2}$$

where L = 90 mm is the length of the D-crystal used in the experiment. For comparison, the CDFDW unit has a maximum vertical acceptance of $\simeq$ 0.15 mm for the same length of the D crystals. This optimization of the vertical acceptance allows us to increase the photon flux delivered by the monochromator.

4. Experimental

The optomechanical design of the monochromator is based on that of the CDFDW optics [31–33]. The Si (022) CFW crystal was replaced by a thin diamond CW crystal with the 133 working Bragg reflection. Requirements on the crystal geometry and orientation are summarized in Fig. 4(a) showing a side and top view sketch of the desired crystal. A small miscut angle $\alpha = 1.5^\circ$ from the (001) crystal plane yields an asymmetry angle $\eta_C = 48^\circ$ for the working Bragg reflection, which is an optimal design value for the CDDW monochromator.

Type IIa diamond single crystals were grown at the Technological Institute for Superhard and Novel Carbon Materials (Troitsk, Russia) using the temperature-gradient method at high static pressure and high temperature (e.g., [26]). After the crystallization process, diamond crystals were cut by a laser from the $\{001\}$ growth sector furthest from the seed and mechanically polished to fabricate crystal plates with a thickness of about 100 μm. The miscut angle α was deliberately introduced and verified after polishing.

#197351 - $15.00 USD Received 16 Sep 2013; revised 30 Oct 2013; accepted 1 Nov 2013; published 9 Dec 2013

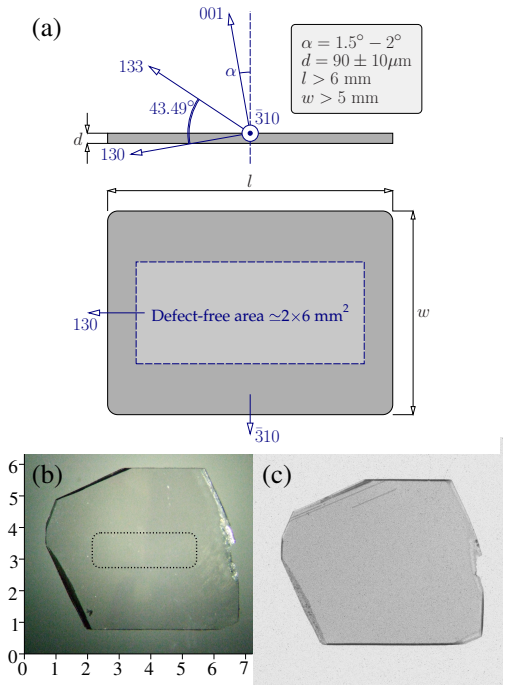

Fig. 4. (a) Side and top view sketch of the desired crystal showing the requirements on diamond (133) crystal geometry and orientation. The arrows and Miller indexes denote reference reciprocal vectors. The miscut angle $\alpha = 1.5^\circ$ from the (001) crystal plane yields the desired asymmetry angle $\eta_C = 48^\circ$ for the working diamond 133 Bragg reflection. (b) A photograph of the diamond crystal with dimensions scale given in mm. The dashed box represents the maximum size of a footprint of an x-ray beam in the working configuration of the monochromator. (c) X-ray Lang topograph of the diamond crystal obtained using C 220 reflection in transmission (Laue) geometry. Crystal orientation in (b) and (c) is the same as in (a) (top view).

White-beam x-ray topography using a laboratory source was performed to determine lattice directions in the crystals. To reveal information about crystal defects and to select the best crystal plate, x-ray Lang topography was performed using an XRT-100 x-ray topography instrument (Rigaku) equipped with an Ag K_α source.

Figure 4(b) shows a photograph of the selected plate. For the incident beam with a cross section of 0.5×1 mm^2, the expected footprint on the diamond is about 3.3×1 mm^2, as shown in Fig. 4(b) by a dashed box (working region).

Figure 4(c) shows a Lang topograph obtained in transmission (Laue geometry) using C 220 reflection. The orientation of the diamond plate as shown in Figs. 4(b) and 4(c) corresponds to that of Fig. 4(a) (top view).

The results of Lang topography suggest an absence of crystal defects in the working region.

Synchrotron experiments were performed at the undulator beamline 30-ID at the Advanced Photon Source at Argonne National Laboratory. To improve heat exchange and the overall thermal stability the entire CDDW monochromator assembly was held in a helium atmosphere. In addition, each D-crystal was placed into an enclosure with a heating element. The heating elements were operated by a control loop feedback mechanism including temperature sensors attached to each D-crystal. During the course of the measurements the temperature of the D

#197351 - $15.00 USD Received 16 Sep 2013; revised 30 Oct 2013; accepted 1 Nov 2013; published 9 Dec 2013

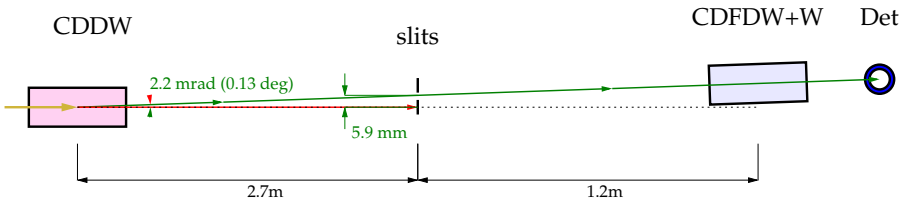

Fig. 5. Scheme of the experimental setup detailing the measurement of the spectral resolution function of the CDDW monochromator using a high-energy-resolution analyzer (CDFDW+W). The scheme shows the setup in the horizontal scattering plane plane. A spatial separation of the eV beam transmitted through the CW diamond crystal (red) and of the monochromatized sub-meV beam (green) is accomplished using angular offsets in $\tilde{\chi}_{D_1}$ and $\tilde{\chi}_{D_2}$. The eV beam is blocked by slits while the sub-meV beam is transmitted through the high-energy-resolution analyzer and measured using a detector (Det).

crystals was controlled with an accuracy of $\approx$ 1 mK (rms) using at least two temperature sensors for each crystal (to ensure uniform temperature distribution). The resulting possible photon energy deviation due to mismatch in temperatures of individual crystals and non-uniform temperature distribution was negligible [$\approx$ 0.04 meV (rms)].

To accommodate the geometrical acceptance of the monochromator (Eq. (2)) and to avoid edge effects, the size of the primary eV beam was limited to 0.3×1.0 mm^2 (vertical $\times$ horizontal) using a slit. The photon flux of the eV beam accepted by the slit was $\approx 1 \times 10^{13}$ photons/s. The slit was placed at a distance of $\approx$ 30 m from the source, which limited the angular divergence of the eV beam to $\approx$ 10 μrad. It is possible that an additional angular divergence originates from small angle scattering of the primary beam from the blades of the slit. The monochromator was placed at a distance of $\simeq$ 37 m from the source. Thus, the design value for the vertical acceptance of the monochromator (0.46 mm) limits the angular spread of the incident beam to a maximum value of $\simeq$ 12 μrad.

The diamond CW crystal diffracts x-ray photons within a 130-meV bandwidth with close-to 100% reflectivity. The rest of the primary incident x-ray beam, having a 0.57-eV bandwidth, is transmitted through the monochromator slightly attenuated by the diamond crystal. The monochromatized x-ray beam (sub-meV beam) resulting from interactions 1-5 (Section 3) propagates in the same direction as the transmitted beam with a vertical offset of only ≈ 100 μm (the thickness of the diamond crystal). The intensity of the sub-meV beam is weaker by more than three orders of magnitude than that of the eV beam. It is clear that in a coplanar diffraction geometry (all reciprocal vectors lie in the same dispersion plane) the two beams will overlap. In order to separate the eV beam and the sub-meV beam, angular offsets in $\tilde{\chi}_{D_1}$ and $\tilde{\chi}_{D_2}$ were introduced, which resulted in a deflection of the sub-meV beam in the horizontal plane as shown in Fig. 5. The eV beam was then blocked by a slit. This non-coplanar geometry is also illustrated in Fig. 2(b).

The angular deviation $\Delta\chi$ of the sub-meV beam from the transmitted eV beam is achieved by variations of angles $\tilde{\chi}_{Dn}$ of the D crystals (n=1,2):

$$\Delta\tilde{\chi}_{Dn} = -\frac{1}{4}\Delta\chi\cos 2\theta_C \tag{3}$$

These variations change the glancing angles of incidence to the reflecting atomic planes, such that the new value $\theta^*_{D_n}$ is related to the old value θ_{D_n} as follows:

$$\sin\theta^*_{D_n} \simeq \sin\theta_{D_n}\cos\Delta\tilde{\chi}_{D_n}. \tag{4}$$

#197351 - $15.00 USD Received 16 Sep 2013; revised 30 Oct 2013; accepted 1 Nov 2013; published 9 Dec 2013

The change in the glancing angles of incidence may result in an energy change of the monochromatized x rays. In our experiment, $\Delta\chi = 2.2$ mrad, $\Delta\tilde{\chi}_{\mathrm{D}n} \simeq 0.2$ mrad and $\Delta\theta_{\mathrm{D}n} \simeq -55$ μrad. The corresponding energy change is only $|\Delta E_0| \simeq 1$ meV.

5. Tuning reflectivity curves

The main tuning curves of the monochromator are shown in Fig. 6 (filled circles, solid lines). Insets in each subfigure show schematically directions of crystal rotations in the angular scans and the path of the x rays to the detector (det). The curves are in a reasonable agreement with theoretical calculations performed in the two-beam approximation (dashed lines). The theoretical calculations were performed under the assumption that all reciprocal vectors of the reflections lie in the dispersion plane.

Figure 6(a) shows an angular dependence of x-ray reflectivity after the first interaction. The FWHM of the curve (93 μrad) is correctly predicted by the theory. This value is larger than the intrinsic width of the asymmetric diamond 133 Bragg reflection ($\Delta\theta_{\mathrm{C}} = \Delta\theta_{\mathrm{C}}^{s}/\sqrt{b_{\mathrm{C}}} \simeq 17.1$ μrad) due to the energy spread of the incident radiation ($\Delta E_X \simeq 0.57$ eV).

Figure 6(b) represents the angular dependence of x-ray reflectivity after the third interaction in the vicinity of exact backscattering from D_1. A drop in intensity is observed in the experimental data in an angular range of about 100 μrad (FWHM). This drop is greater than the one predicted using the two-beam approximation. The approximation takes into account only one channel for x-ray intensity loss, the diamond 133 reflection of the beam backscattered from the D_1 crystal, as shown by the gold arrow in the inset of Fig. 6(b). The larger observed intensity drop can be attributed to additional losses due to multiple-beam diffraction in backscattering. In order to avoid such losses, a positive angular offset from the exact backscattering $\delta\tilde{\Theta}_{\mathrm{D}_1} \approx 200$ μrad was introduced, as illustrated by the green-filled arrow in the figure.

Figure 6(c) shows x-ray reflectivity from all crystals of the CDDW monochromator as a function of $\tilde{\Theta}_{\mathrm{D}_2}$. Measurement of this curve serves as a confirmation for the presence of the sub-meV beam passed through the monochromator and is the final step in the alignment procedure.

Figure 6(d) shows x-ray reflectivity from all crystals of the monochromator as a function of the common rotation angle $\tilde{\theta}$, thus representing the angular acceptance of the monochromator for the eV beam. The resulting angular width of the curve ($\simeq 21$ μrad) can be understood as a convolution of the intrinsic angular acceptance of the first reflection ($\simeq 17$ μrad) and the angular divergence of the incident eV beam (≈ 12 μrad).

Energy tuning of the monochromator is accomplished by the simultaneous rotation of the D crystals in opposite directions as shown in the inset of Fig. 7, in the same way as for the CDFDW optics [18]. The relationship between the angular and the energy scales is given by

$$\delta\Theta = \frac{\delta E}{E_0}\tan\eta_{\mathrm{D}}, \tag{5}$$

where $\delta\Theta$ and δE are accordingly angular and energy deviations from the exact backscattering [18]. The measured angular tunability range of the monochromator is 57 μrad (FWHM), which corresponds to an energy range of $\simeq 18.2$ meV. This is shown by the second x-axis scale in Fig. 7 in units of photon energy. The total energy tunability range can be increased by varying the temperature of the D crystals.

6. Spectral resolution function

This section provides details on the measurement of the spectral resolution function of the CDDW monochromator. A scheme of the experimental setup in the dispersion (vertical) plane is shown in Fig. 8(a). The energy bandwidth of the monochromator was evaluated using an existing CDFDW unit in combination with a Si (022) channel-cut crystal (+W). The use of a +W

#197351 - $15.00 USD Received 16 Sep 2013; revised 30 Oct 2013; accepted 1 Nov 2013; published 9 Dec 2013

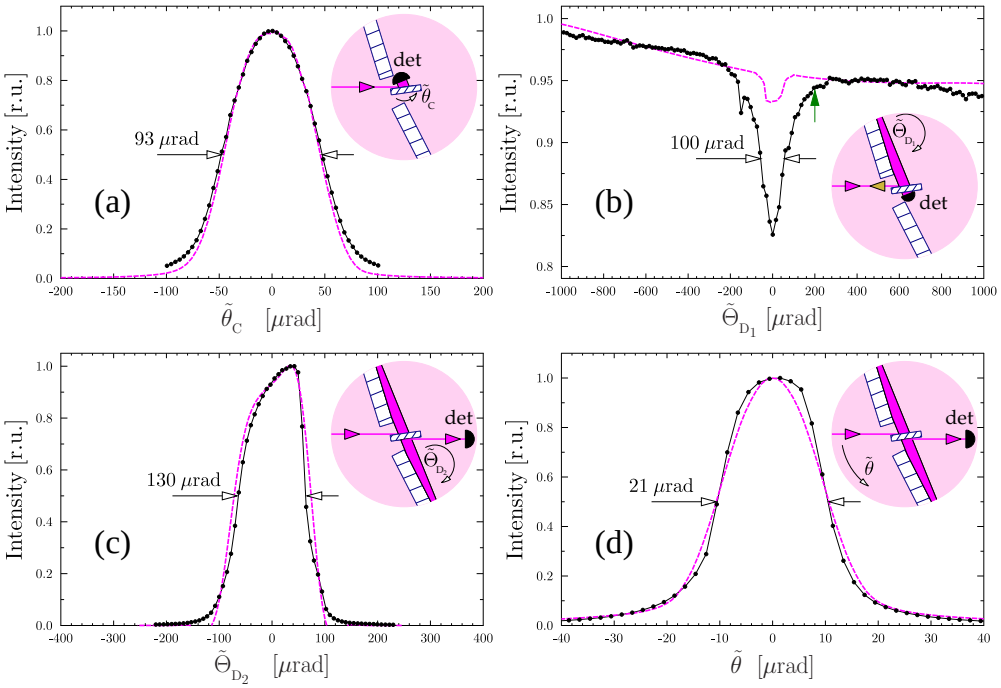

Fig. 6. Main tuning curves of the CDDW monochromator (filled circles and solid lines), representing angular dependencies of reflectivity of x rays: (a) from the CW crystal, as a function of $\tilde{\theta}_C$; (b) from the CW crystal, from the D_1 crystal, and transmission through the CW crystal, as a function of $\tilde{\Theta}_{D_1}$; (c) from all crystals of the CDDW monochromator (i.e., after all five interactions) as a function of $\tilde{\Theta}_{D_2}$; (d) from all crystals of the CDDW monochromator as a function of $\tilde{\theta}$. The last curve represents the angular acceptance of the CDDW monochromator for the eV beam. The dashed lines show results of numerical calculations using the dynamical theory of x-ray diffraction in the two-beam approximation. The insets in each subfigure show schematically the directions of crystal rotations in the angular scan and the path of the x rays to the detector (det). To avoid intensity losses due to proximity to exact backscattering, an angular offset $\delta\tilde{\Theta}_{D_1} \approx 200$ μrad was applied as shown in (b) by the green-filled arrow. The gold arrow in the inset of (b) shows the x-ray beam reflected consecutively from the D_1 crystal in backscattering and backwards from the diamond crystal

.

element allows us to select a narrow bandwidth of $\Delta E \simeq 0.1$ meV from the energy bandwidth of CDFDW ($\Delta E \simeq 0.4$ meV) [21]. The experimentally measured curve is shown in Fig. 8(b) (filled circles). A theoretical curve (solid line) was calculated using a convolution of the spectral distribution functions of the monochromator and the CDFDW +W analyzer. The spectral bandwidths of the two curves match with good accuracy. The bandwidth of the spectral resolution function of the CDDW monochromator can be estimated assuming that the CDFDW +W analyzer has a theoretical bandwidth of 0.08 meV and that the two can be added in quadrature to yield the measured value of 0.263 meV. The resulting bandwidth $\Delta E_M = 0.25 \pm 0.01$ meV (FWHM) is consistent with the theoretical value (0.246 meV).

A Gaussian (dashed line) and a Lorentzian (dash-dotted line) functions with the same FWHM are plotted for comparison. The spectral tails of the resolution function are only slightly worse than those predicted by the theory, yet about an order of magnitude steeper than those of the

#197351 - $15.00 USD Received 16 Sep 2013; revised 30 Oct 2013; accepted 1 Nov 2013; published 9 Dec 2013

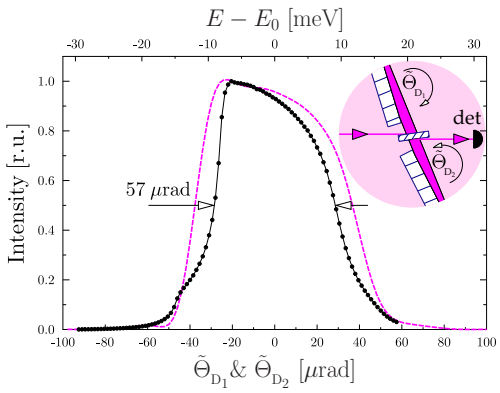

Fig. 7. Energy tuning curve of the CDDW monochromator (solid circles and lines) performed by simultaneous variation of angles $\tilde{\Theta}_{D_1}$ and $\tilde{\Theta}_{D_2}$ (as shown in the inset) The dashed line shows the result of numerical calculations using dynamical theory of x-ray diffraction in the two-beam approximation.

Lorentzian function at an offset of a few meV from the peak. This is particularly important in inelastic x-ray scattering experiments to resolve low-intensity inelastic features in the proximity to the elastic line. The measured resolution function suggests that the spectral function of the monochromator provides a dynamic range of $\approx 10^3$ at an energy offset of about 2 meV (i.e., high spectral contrast).

7. Spectral efficiency and delivered photon flux

Another important characteristic of the performance of the monochromator is the spectral efficiency:

$$\varepsilon_M = \frac{I_M}{I_X}\frac{\Delta E_X}{\Delta E_M}. \tag{6}$$

Here, I_X is the photon flux of the incident eV beam, I_M is the photon flux of the sub-meV beam, and $\Delta E_X/\Delta E_M$ is the ratio of their energy bandwidths. The spectral efficiency given by Eq. (6) is not to be confused with the theoretical peak throughput, which is $T \simeq 58\%$ (see Fig. 3). The theoretical spectral efficiency is $\varepsilon_M \simeq 68\%$. The measured value $\simeq 65$ % was slightly lower that the theoretical prediction, which can be attributed to crystal imperfection. Still, it is exceptionally high compared with that of the existing high-energy-resolution multicrystal monochromators (e.g., [11, 34–38]).

The measured photon flux of the sub-meV beam after the monochromator was 1.8×10^9 photons/s with the nominal incident eV beam size of 0.3×1.0 mm^2 (vertical $\times$ horizontal). With an increase in the incident beam size an increase in the delivered flux was obtained up to 3.3×10^9 photons/s, however, the spectral efficiency dropped to $\simeq 52$ %.

8. Summary and conclusions

The design and measured performance parameters of the CDDW monochromator are summarized in Table 2.

In conclusion, we have designed, built, and evaluated a hybrid diamond-silicon angular-dispersive x-ray monochromator, which can be used for high-energy-resolution inelastic x-ray scattering. It has an energy resolution of $\Delta E \simeq 0.25$ meV and spectral efficiency of 65 %. The monochromator utilizes x rays with a photon energy of ≈ 9 keV. Therefore, it is applicable both at high-energy and at medium-energy storage ring synchrotron radiation facilities,

#197351 - $15.00 USD Received 16 Sep 2013; revised 30 Oct 2013; accepted 1 Nov 2013; published 9 Dec 2013

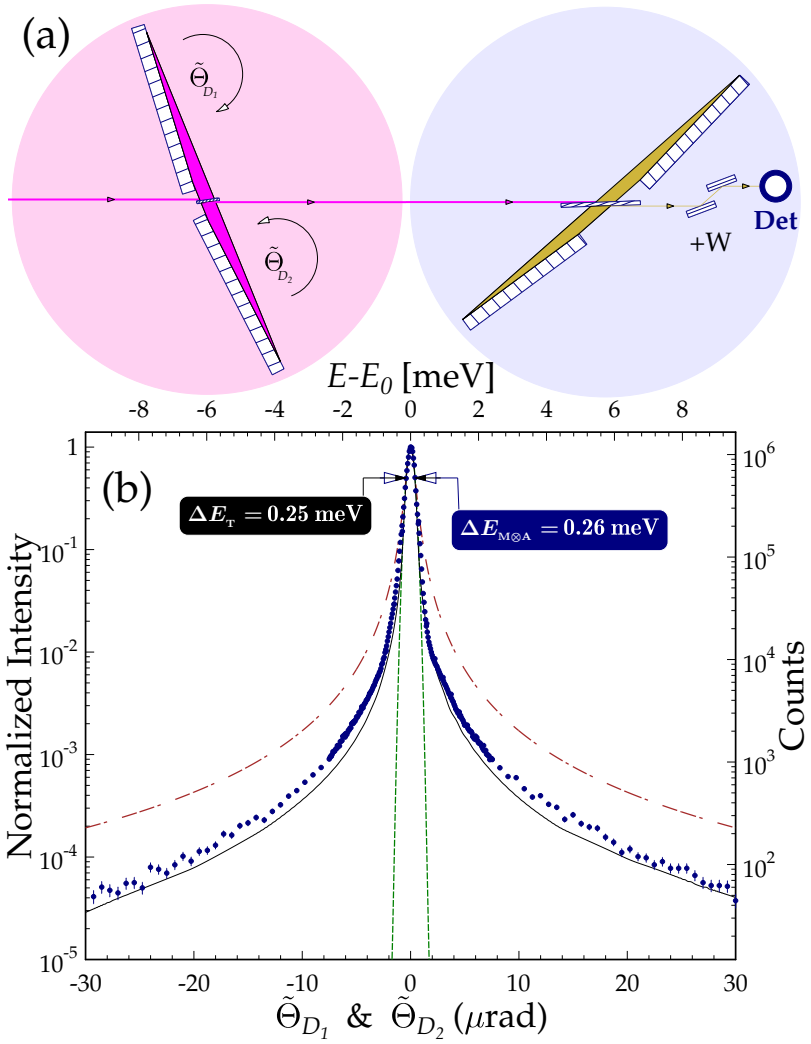

Fig. 8. (a) Scheme of the experimental setup in the dispersion (vertical) plane. (b) Spectral resolution function of the CDDW monochromator against CDFDW +W analyzer. The experimental spectral resolution function is shown by filled circles; the black solid line shows spectral resolution function calculated using the dynamical theory of x-ray diffraction. Other functions with the same FWHM are shown for comparison: Gaussian (dashed line) and Lorentzian (dash-dotted line).

as well as at XFEL facilities. The operation of the monochromator is based on the effect of angular dispersion in Bragg diffraction from asymmetrically cut crystals. It does not rely on the intrinsic energy widths of Bragg reflections. This, in combination with a choice of low absorbing diamond crystal for a collimator/wavelength selector, allows us to overcome the energy resolution *versus* efficiency trade-off of conventional high-energy-resolution x-ray optics. The demonstrated spectral efficiency of the monochromator is particularly remarkable considering the small spectral bandwidth and the operating x-ray energy.

Other advantages of the monochromator in comparison to the CDFDW optics implemented earlier are the 3-fold increase in the aperture of the accepted beam and the reduction in the cu-

#197351 - $15.00 USD Received 16 Sep 2013; revised 30 Oct 2013; accepted 1 Nov 2013; published 9 Dec 2013

Table 2. Design and measured parameters of the CDDW monochromator: ΔE_M, FWHM of the spectral resolution function; δE_M, accessible energy range (FWHM) provided by angular tunability (Eq. (5)); $\Delta\theta_M$, angular acceptance; V, maximum (theory) and nominal (experiment) vertical acceptance; ε_M, spectral efficiency [Eq. (6)]; and I_M, delivered photon flux at the 30-ID undulator beamline with the incident beam cross section of 0.3×1.0 mm^2.

	ΔE_M (meV)	δE_M (meV)	$\Delta\theta_M$ (μrad)	V (mm)	ε_M (%)	I_M (ph/s)
Theory	0.246	23.5	17	0.46	68	-
Experiment	0.25	18.2	17	0.32	65	1.8×10^9

mulative angular dispersion rate of the outgoing x rays for better focusing on a sample. The angular acceptance of the CDDW monochromator ($\simeq 17$ μrad) is about five times smaller than the angular acceptance of the CDFDW optics. However, it perfectly matches the angular divergence of an undulator source. The measured performance parameters of the monochromator are suitable for non-resonant inelastic x-ray spectroscopy with an absolute energy resolution < 1 meV and other high-energy-resolution applications.

Finally, we demonstrate a working application of the state-of-the-art diamond crystal technology in high-resolution x-ray optics. Physical properties of diamond, such as high thermal conductivity, low thermal expansion, low x-ray absorption, and high radiation hardness make it a preferable material for x-ray optics at synchrotrons and XFELs. Due to the choice of a thin diamond crystal as the primary crystal, operation of the monochromator is feasible with the intense self-seeded incident XFEL beam [29] in beam-sharing mode [39]. The monochromator does not transmit photons within a narrow energy band of ≈ 105 meV (the intrinsic energy width of the first reflection), which is smaller than the energy width of the self-seeded x-ray beam (≈ 0.5 eV). The photons outside of the narrow energy band are transmitted through the diamond crystal (≈ 50 % transmission at 9.13 keV) and can be delivered to the next experimental station. The transmission can be improved using thinner diamond crystals.

Acknowledgments

We are grateful to L. Young for support of this project at the Advanced Photon Source. We thank T. Roberts, K. Goetze, J. Kirchman, R. Krakora, W. Jansma, and S. Ross for help with instrumentation and controls. J. Kim, M. Upton, and Y. Ding are acknowledged for technical support of the experiment. The present work was supported through a research grant from the Russian Ministry of Education and Science (Contract Nos.16.552.11.7014). Use of the Advanced Photon Source, an Office of Science User Facility operated for the U.S. Department of Energy (DOE) Office of Science by Argonne National Laboratory, was supported by the U.S. DOE under Contract No. DE-AC02-06CH11357.